Molecular Dynamics and Continuum Electrostatics Studies of Inactivation in the HERG Potassium Channel

Ramzi Kutteh,*,† Jamie I. Vandenberg,‡,§ and Serdar Kuyucak†

School of Physics, University of Sydney, Sydney, New South Wales 2006, Australia, Mark Cowley Lidwill Research Program in Cardiac Electrophysiology, Victor Chang Cardiac Research Institute, 384 Victoria Street, Darlinghurst, New South Wales 2010, Australia, and St Vincent's Clinical School, University of New South Wales, Darlinghurst, New South Wales 2010, Australia

Received: September 25, 2006; In Final Form: November 9, 2006

Fast inactivation of the HERG potassium channel plays a critical role in normal cardiac function. Malfunction of these channels due to either genetic mutations or blockade by drugs leads to cardiac arrhythmias. An unusually long S5-P linker in the outer mouth of HERG is implicated in the fast inactivation mechanism. To examine the role of the S5-P linker in this inactivation mechanism, we study the permeation properties of the open and inactive states of a recent homology model of HERG. This model was constructed using the KcsA potassium channel as a template and contains specific conformations of the S5-P linker in the open and inactive states. We perform molecular dynamics simulations on the HERG model, followed by free energy, structural, and continuum electrostatics calculations. Our free energy calculations lead to selectivity results of the model channel (K^+ over Na^+) that are different in some respects from those of other potassium channels but consistent with experimental observations. Our structural results show that, in the inactive state, the S5-P linkers move closer to the channel axis, possibly causing a steric hindrance to permeating K^+ ions. Our electrostatics calculations reveal, in the inactive state, an electrostatic potential energy barrier of approximately 14 kT at the extracellular pore entrance, again sufficient to stop K^+ ion permeation through the pore. These results suggest that a steric and/or electrostatic plug mechanism contributes to inactivation in the HERG homology model.

1. Introduction

The human ether-a-go-go related gene (HERG) encodes the pore-forming subunit that conducts the rapid component of the delayed rectifier current I_{Kr}.[1] HERG is a member of the family of voltage-gated potassium (K_V) channels. Each channel consists of four identical subunits and, as shown in Figure 1, each subunit comprises six transmembrane domains. The role of HERG channels has been best characterized in cardiac tissues, where they contribute to normal cardiac repolarization.[2,3] (For a review of the physiology of HERG, see ref 4.) Loss of function mutations in HERG have been linked to the long-QT syndrome,[1,5] the most common inherited primary arrhythmia syndrome, and gain of function mutations in HERG cause the short-QT syndrome.[6] In addition, blockade of HERG by several common drugs causes drug-induced long-QT syndrome.[7,8] There is therefore considerable interest in understanding the structure−function relationship in HERG channels.

Voltage-gated potassium channels can exist in at least three different gating states: the closed state, open state, and inactivated state (an open but nonconducting state).[9] In comparison to other K_V channels, HERG has rather unusual gating properties.[9,10] First, transitions between the open and the closed states (activation/deactivation) are considerably slower than transitions between the open and the inactive states (inactivation/recovery from inactivation). Time constants for activation are on the order of 10^2-10^3 ms, whereas time constants for inactivation are on the order of 1−10 ms; i.e., inactivation is approximately 100 times faster than activation. By comparison, in Shaker K^+ channels the time constant of activation is on the order of 10 ms, whereas the time constant of C-type inactivation is on the order of 10^3 ms.[9] Second, HERG inactivation is voltage-dependent.[2,3] The origin of this voltage dependence is controversial.[10,11]

From fluorescence measurements of fluorophores attached to the N-terminal end of the fourth transmembrane (S4) domain of HERG[12] and gating charge measurements,[11] it was found that the slow activation kinetics was due to the slow movement of the S4 domain. These fluorescence and gating charge experiments[11,12] also revealed voltage-dependent changes in protein conformation that occurred on a millisecond time scale. However, the voltage range over which the rapid conformational changes took place was not consistent with the voltage dependence of HERG inactivation. Thus the origin of the voltage dependence of HERG inactivation remains unresolved. Mutagenesis studies have shown that at least two regions of the channel contribute to inactivation: the pore helix and selectivity filter[2,13−15] and the linker between the S5 domain and the pore helix, the so-called S5-P linker.[16,17] The S5-P linker in HERG is relatively long (approximately 40 amino acids compared to 10−15 amino acids in most K_V channels).[16,18] Recent NMR studies of the S5-P linker have shown that while it does not have discernible motifs in water it does display two well-defined helical regions in the presence of sodium dodecyl sulfate (SDS) micelles[17] or dipalmitoyl phosphatidylcholine (DPC) micelles.[19]

* Author to whom correspondence should be addressed. E-mail: r.kutteh@mailaps.org.
† University of Sydney.
‡ Victor Chang Cardiac Research Institute.
§ University of New South Wales.

10.1021/jp066294d CCC: $37.00
Published on Web 01/18/2007

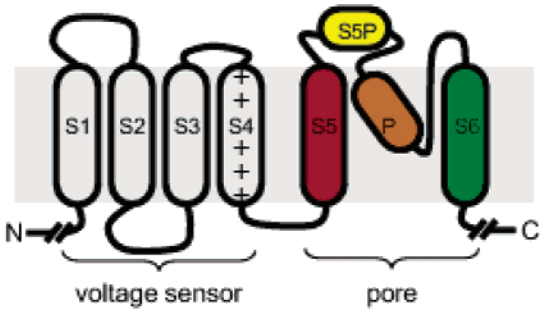


```
Shaker   LKASMRELGLLIFFLFIGVVLFSSAVYFAEAGSEN---------------------------- 423
Kv21     LRRSYNELGLLILFLAMGIMIFSSLVFFAEKDEDD---------------------------- 354
Kv43     LKSCASELGFLLFSLTMAIIIFATVMFYAEKGSSA---------------------------- 348
KvAP     DAADKIRFYHLFGAVMLTVLYGAFAIYIVEYPDPN---------------------------- 190
KcsA     SALHWRAAGAATVLLVIVLLAGSYLAVLAERGAPG---------------------------- 56
MtHK     PRVLKVPATRILLLVLAVIIYGTAGFHFIEG-------------------------------- 121
HERG     YSEYGAAVLFLLMCTFALIAHWLACIWYAIGNMEQPHMDSRIGWLHNLGDQIGKPYNSSGLGGP 605

Shaker   SFFKSIPDAFWWAVVTMTTVGYGDMTPVGVWGKIVGSLCAIAGVLTIALPVPVIVSNFNYFYHR 487
Kv21     TKFKSIPASFWWATITMTTVGYGDIYPKTLLGKIVGGLCCIAGVLVIALPIPIIVNNFSEFYKE 418
Kv43     SKFTSIPASFWYTIVTMTTLGYGDMVLKTIAGKIFGSICSLSGVLVIALPVPVIVSNFSRIYHQ 412
KvAP     SSIKSVFDALWWAVVTATTVGYGDVVPATPIGKVIGIAVMLTGISALTLLIGTVSNMFQKILVG 254
KcsA     AQLITYPRALWWSVETATTVGYGDLYPVTLWGRLVAVVVMVAGITSFGLVTAALATWFVGREQE 120
MtHK     ---ESWTVSLYWTFVTIATVGYGDYSPSTPLGMYFTVTLIVLGIGTFAVAVERLLEFLINREQM 182
HERG     SIKDKYVTALYFTFSSLTSVGFGNVSPNTNSEKIFSICVMLIGSLMYASIFGNVSAIIQRLYSG 669
```

Figure 1. (Top) Two-dimensional transmembrane topology of a voltage-gated potassium (K_V) channel subunit, showing the six transmembrane domains S1−S6, the pore helix (P), and the S5-P extracellular linker. The computational studies in this work focus on a homology model of the pore region (S5−S6) of HERG. (Bottom) Alignment of amino acid sequences from the start of S5 (red band) to the end of S6 (green band) of HERG and other potassium channels. For KcsA (also examined in this work), S5 and S6 correspond to its two domains. The yellow band marks the S5-P linker, and the orange band marks the pore helix.

A partial helical structure for S5-P is also suggested from cysteine-scanning mutagenesis experiments.[16]

These findings give valuable hints about the operation of the HERG channel. However, it is very difficult to infer the structure of the channel from such experiments alone. Determination of the crystal structure of eukaryotic channel proteins is a difficult problem, and it is unlikely that an experimental molecular structure for HERG will be available in the near future. An alternative method that complements the experimental work is to explore the gating properties of the channel through molecular modeling and computation. Such computational studies can provide a direct link between the channel structure and its function, which is the main goal of all work in the field. Availability of several crystal structures for potassium channels (e.g., KcsA,[20,21] MthK,[22] and KvAP[23]) makes this alternative computational approach easier. Already several homology models of HERG have been constructed using the crystal structures of the bacterial potassium channels, such as KcsA,[24,25] MthK,[26] and KvAP.[27,28] The focus of these studies was drug binding and blocking of the channel from the intracellular side. Consequently not much attention was paid to the S5-P linker structure on the extracellular side and the inactivation mechanism associated with it. However, a homology model of HERG that describes specifically the S5-P linker conformations in the open and inactive states has been recently constructed from the KcsA structure,[29] but its functional properties have not been studied yet.

Here we use this HERG homology model and molecular dynamics (MD) simulations to construct and equilibrate systems corresponding to the open and inactive states of the HERG channel. The validity of the model is then assessed with calculations of the relative binding free energies of Na^+ and K^+ to the channel pore. Free energy results are compared to those from analogous calculations we performed on a KcsA system, and the computed selectivity of the HERG model is interpreted in terms of experimental data. After model validation, structural and continuum electrostatics calculations are performed on configurations from the equilibrated HERG systems to compute average pore radii along the channel axis, molecular surfaces, electrostatic potential and potential energy profiles along the channel axis, and potentials mapped to molecular surfaces. The results of these calculations are used to study the suitability of this homology model for describing the permeation properties of the open and inactive states in HERG. In particular, we address the important question of whether the inactivation can be achieved by a steric and/or electrostatic barrier mediated by the S5-P linker or whether conformational changes in the selectivity filter are necessary for that purpose.

2. Model Systems and Methods

2.1. Construction and Equilibration of the Systems. Using the aforementioned homology model of HERG,[29] two simulation systems are constructed using the VMD package:[30] one for the channel in the open state and another in the inactive state. As shown in Figure 2, the selectivity filter of the HERG channel is formed by the residue sequence SVGFG (residues Ser624 to Gly628), which differs from the TVGYG signature sequence of other potassium channels (Figure 1). To distinguish between different filter occupancy states, we adopt henceforth the

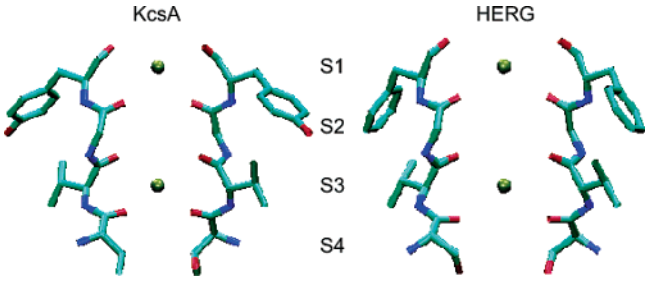

Figure 2. Selectivity filters of KcsA (TVGYG) and the HERG homology model (SVGFG) prior to equilibration with K^+ ions occupying the binding sites S1 and S3. The water molecules in sites S2 and S4 are not shown. Only two subunits are displayed for clarity.

notation of Luzhkov and Aqvist,[31] where "1" designates a binding site occupied by a K^+ ion and "0" designates a site occupied by a water molecule. Hence (1010) denotes a filter occupancy state where sites S1 and S3 are occupied each by a K^+ ion while sites S2 and S4 are occupied each by a water molecule. In addition, a third K^+ ion is always present in the internal cavity in all of our calculations. Initially, a bilayer of palmitoyl oleoyl phosphatidyl ethanolamine (POPE) molecules with 86 lipids per layer is constructed in an $x-y$ area of 80×80 Å ^{2}. Homology models of HERG in the open and inactive structures, with filter occupancy state (1010) (TIP3P water molecules in sites S2 and S4), are each embedded in the middle of a membrane bilayer. Each protein/membrane complex is then solvated with TIP3P waters in a box with the same $x-y$ dimensions of 80×80 Å^2, but extending 15 Å above and below the membrane in the $+z$ and $-z$ directions. This corresponds to five layers of water molecules between the lipid bilayer and the simulation box surface, which is sufficient for avoiding simulation artifacts arising from periodicity.[32] Water is then removed from the hydrophobic inside of the membrane (except the filter region). As the homology model of HERG has $+4e$ charge (without the three K^+ ions), each system is then ionized with seven Cl^- ions to maintain total charge neutrality.

The two HERG systems, constructed as described above, are next equilibrated with MD simulations carried out using the NAMD code[33] with the CHARMM 27 force field,[34] which provides a complete set of parameters for all the atoms in the system. An NPT ensemble is used with periodic boundary conditions. Electrostatic interactions are computed using the particle mesh Ewald algorithm. A time step of 2 fs is employed for all simulations. A switching distance of 8.5 Å and a cutoff distance of 10 Å are used for Lennard-Jones interactions. The list of nonbonded interactions is truncated at 11.5 Å and updated every 20 steps. First, energy minimization is performed on each system for 10 000 steps, keeping all protein backbone atoms and the three K^+ ions fixed. Further energy minimization is performed for an additional 10 000 steps, with all protein backbone atoms and the three K^+ ions harmonically restrained with force constants of 10 kcal/mol/Å^2. Each system is then heated to 298 K with a Langevin damping coefficient of 10 ps^{-1} for 200 ps. A pressure of 1 atm is then applied with a Langevin piston[35] in all three directions until (for approximately 1 ns) the $x-y$ area of each system has converged to the experimental lipid density of ~60 Å^2 per lipid molecule.[36] At this stage the periodic box is fixed in the x and y directions, a pressure coupling of 1 atm is applied in the z direction only, and the system is equilibrated for a further 400 ps. The harmonic restraints on the protein backbone atoms are then reduced to 1 kcal/mol/Å^2, and each system is equilibrated for a further 800 ps. To maintain the desired filter occupancy state, the harmonic restraints on the three K^+ ions are kept at 10 kcal/mol/Å^2 for

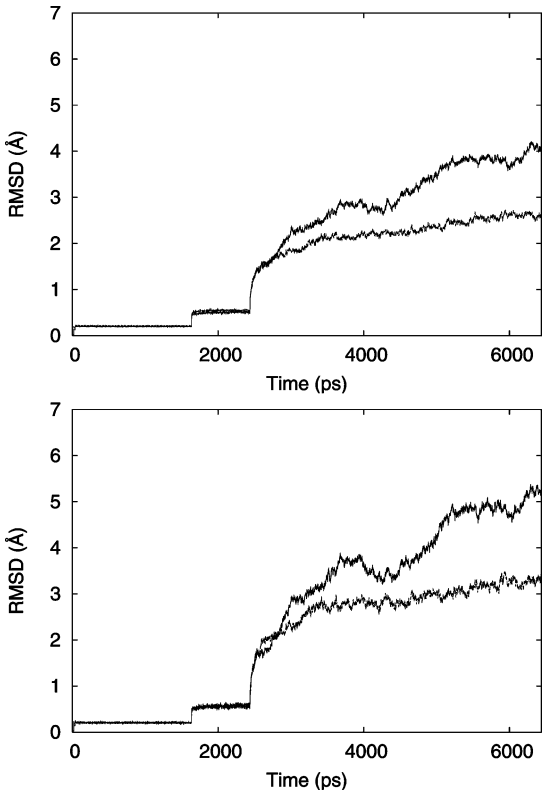

Figure 3. (Top) Root-mean-square deviations of the backbone atoms of HERG (residues Tyr545 to Thr670) from the initial homology models during equilibration. (Bottom) The same quantities plotted for the S5-P linker (residues Ala570 to Tyr611) backbone atoms only. In both panels, the lower curves correspond to the inactive structure, and the upper curves correspond to the open one.

the remainder of the equilibration. Finally, the harmonic restraints on the protein backbone atoms are removed, and each system is equilibrated for an additional 4 ns. One indicator of equilibration is the saturation with time in the root-mean-square deviation (rmsd) from the initial configuration of the system, as shown in Figure 3. Snapshots of the open and inactive HERG structures at the end of equilibration are shown in Figure 4.

We have experimented with other less stringent equilibration protocols (e.g., keeping only the protein C_α atoms harmonically restrained rather than the backbone atoms) but found the one described above necessary to prevent distortion in the filter structure during the early stages of equilibration. The two equilibrated systems, corresponding to the open and inactive HERG structures with filter occupancy state (1010), form the basis of the electrostatic and structural calculations. For the free energy calculations we require instead two equilibrated systems both corresponding to the open HERG structure but with filter occupancy states (1010) and (0101). The latter is obtained from the former with the appropriate interchanges in water and K^+ ion positions in the filter binding sites, followed by equilibration for 400 ps, maintaining the same values for all simulation parameters. Free energy calculations were also performed on two equilibrated systems of the KcsA potassium channel with filter occupancy states (1010) and (0101). As shown in Figure 2, the selectivity filter of the KcsA channel is formed by the signature residue sequence TVGYG (residues Thr75 to Gly79). Starting with the KcsA crystallographic structure obtained at 2 Å resolution,[21] the two equilibrated systems were generated by the same procedure described above for the HERG systems, although a less stringent equilibration protocol was feasible for

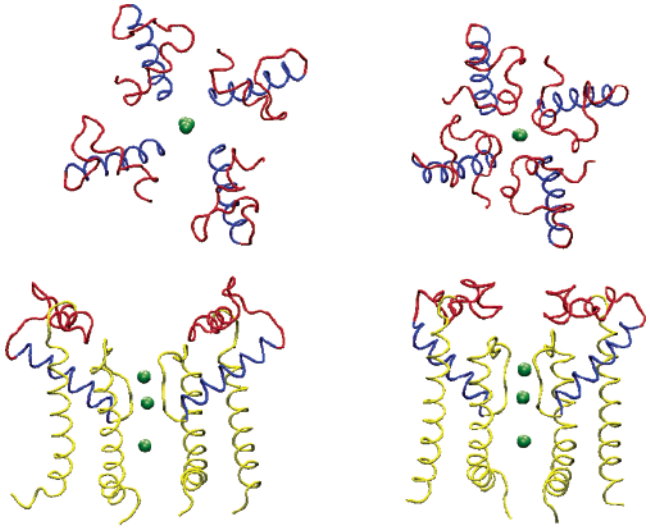

Figure 4. Structure of the open (left) and inactive (right) states in HERG after equilibration with K^+ ions (lime) in sites S1, S3, and the internal cavity. The top panels show the top view of the S5-P linkers (red, residues His578 to Gly604) and pore helices (blue, residues Pro605 to Leu622) from the extracellular side. The bottom panels show the cross-sectional view of the channel inside the lipid bilayer, including the S5 helices (yellow, residues Tyr545 to Pro577) and the filter−PS6−S6 regions (yellow, residues Thr623 to Thr670). Only two of the four monomers are shown in the bottom panels for clarity.

KcsA, as its structure displays a higher degree of stability during simulation than that of the HERG homology model.

2.2. Relative Binding Free Energies to the Channel Pore. The selectivity of the HERG channel is controlled by the narrow filter region formed by the residue sequence SVGFG (residues Ser624 to Gly628), as depicted in Figure 2. To examine the selectivity property of the HERG homology model, we determine the relative binding free energy of Na^+ and K^+ to the channel pore, $\Delta\Delta G$, which is the difference between the binding free energies of Na^+ and K^+. Specifically,

$$\begin{aligned}\Delta\Delta G &= [G_p(Na^+) - G_w(Na^+)] - [G_p(K^+) - G_w(K^+)] \\ &= \Delta G_{bind}(Na^+) - \Delta G_{bind}(K^+) \\ &= \Delta G_p(K^+ \rightarrow Na^+) - \Delta G_w(K^+ \rightarrow Na^+) \end{aligned} \quad (1)$$

where $\Delta G_p(K^+ \rightarrow Na^+)$ and $\Delta G_w(K^+ \rightarrow Na^+)$ represent the mutation free energies of K^+ into Na^+ in the protein and water, respectively, and the last equality follows from standard thermodynamic cycle arguments.[37] A positive value for $\Delta\Delta G$ implies selectivity for K^+ over Na^+. To determine $\Delta\Delta G$, the popular free energy perturbation (FEP) method[37,38] is employed to compute $\Delta G_p(K^+ \rightarrow Na^+)$ and $\Delta G_w(K^+ \rightarrow Na^+)$ by transforming or mutating a K^+ ion in the selectivity filter or bulk water into a Na^+ ion.

The FEP approach is based on Zwanzig's "perturbation formula" for the free energy difference between the initial state A and the final state B of a system

$$\Delta G(A \rightarrow B) = -kT \ln \langle \exp[-(H_B - H_A)/kT] \rangle_A \quad (2)$$

where the ensemble average is performed over configurations representative of state A (i.e., generated with the Hamiltonian H_A). Interchanging the final and initial states, eq 2 becomes by symmetry

$$\Delta G(B \rightarrow A) = -kT \ln \langle \exp[-(H_A - H_B)/kT] \rangle_B \quad (3)$$

Equations 2 and 3 are referred to as the forward and backward free energy differences. As free energy is a state function, we should in principle have $\Delta G(A \rightarrow B) = -\Delta G(B \rightarrow A)$. In practice, however, the values of $\Delta G(A \rightarrow B)$ from eqs 2 and 3 differ by the so-called hysteresis of the computation. To improve accuracy, double-ended sampling is usually performed by calculating $\Delta G(A \rightarrow B)$ with both equations and taking the average.

To obtain accurate results with eq 2, at least two criteria must be observed in FEP calculations:[38,39] (a) one must sample for a sufficiently long time for the ensemble average to converge, and (b) states A and B must be similar enough that the ensemble of configurations generated for A is also representative of B. If states A and B differ substantially, then the ensemble of configurations generated for A will not be very representative of B. In this case, given that the configurations generated for state A will be predominantly low-energy configurations of A, they will be predominantly high-energy configurations of B, leading to large positive values for $(H_B - H_A)$ or small values for $\exp[-(H_B - H_A)/kT]$. Such small values in the ensemble average are easily dominated by truncation and round-off errors, leading to poor convergence in eq 2. To obtain accurate results with eq 2, the free energy difference between states A and B must be roughly less than 2 kT.[37,38] However, in most biochemical processes the free energy change is much larger than that. In order to address (b) then, one introduces a hybrid Hamiltonian of the system

$$H(\lambda) = (1 - \lambda)H_A + \lambda H_B \quad (4)$$

where λ is a coupling parameter that labels intermediate nonphysical states between the initial state A ($\lambda = 0$) and the final state B ($\lambda = 1$). The interval between $\lambda = 0$ and 1 is divided into n windows, using $\{\lambda_0 = 0, \lambda_1, \lambda_2, ..., \lambda_n = 1\}$. For each window, the free energy difference is calculated as in eq 2

$$\Delta G(\lambda_i \rightarrow \lambda_{i+1}) = -kT \ln \langle \exp[-(H(\lambda_{i+1}) - H(\lambda_i))/kT] \rangle_{\lambda_i} \quad (5)$$

and the total free energy change is obtained by summing the contributions from the individual windows

$$\Delta G(A \rightarrow B) = \sum_{i=0}^{n-1} \Delta G(\lambda_i \rightarrow \lambda_{i+1}) \quad (6)$$

Therefore in FEP, $\Delta\Delta G$ is computed by applying eq 6 to $\Delta G_p(K^+ \rightarrow Na^+)$ and $\Delta G_w(K^+ \rightarrow Na^+)$ in eq 1.

2.3. Electrostatic Calculations. The code DelPhi[40,41] is used with the open and inactive structures of HERG to compute three electrostatic quantities: the electrostatic potential profiles along the channel axis, the potential maps (phimaps) of the systems, and the electrostatic potential energy profiles of a test K^+ ion approaching the pore from the extracellular side along the channel axis. To generate the potential profiles, we first obtain a molecular configuration from either of the two equilibrated systems described in section 2.1, corresponding to the open or inactive HERG structures with filter occupancy state (1010). All water molecules and chloride ions (initially added for total charge neutrality) are extracted from the PDB file of this configuration, leaving the protein/membrane complex (including the three potassium ions). The reduced PDB file is then fed into DelPhi to compute the electrostatic potential profile along the channel axis of the configuration. DelPhi places the protein/membrane complex in a cubic grid box and treats it as a single dielectric object. The remainder of the volume in the box is

occupied by a continuum solvent, which is taken here to be water. First, the molecular surface of the dielectric object is computed using the CHARMM Van der Waals radii of the atoms. Using this dielectric/solvent boundary and the CHARMM partial charges for all atoms, DelPhi then solves the Poisson equation iteratively with a finite difference algorithm. Because the Van der Waals radii and partial charges of protein atoms only are provided with DelPhi, we extracted for our purposes the Van der Waals radii and partial charges of all POPE lipid membrane atoms from the CHARMM parameter and topology files, respectively.

For the dielectric constants of the protein/membrane complex and water, the typical values of 4 and 80, respectively, are used. A convergence threshold value of 10^{-4} kT/e (T = 298 K) is imposed, based on the maximum change of grid potential between successive iterations. The number of grid points on each side of the cubic lattice was chosen to be 285. To have accurate boundary conditions on the sides of the grid box while simultaneously employing a sufficiently fine grid for an accurate calculation of the potential, a two-run focusing strategy[42] is adopted in all of our DelPhi calculations. In the first run, the largest linear dimension of the protein/membrane complex is scaled to 45% of the side of the grid box (i.e., resolution of 1.45 grid points per Å), and dipolar boundary conditions are used. In the second run, the largest linear dimension of the protein/membrane complex is scaled to 65% of the side of the box (i.e., resolution of 2.1 grid points per Å), and the boundary conditions are calculated by interpolation from the potentials computed in the first run. To generate the electrostatic potential profile along the axis of a channel structure, we need the potential at all grid points at the end of this second run. To this end, we output from DelPhi a table of the potential at all grid points. The (x,y) coordinates of the channel axis are obtained by averaging the x and y coordinates of the two K^+ ions in the channel filter. We then select from this table the grid line parallel to the z-axis and with the nearest (x,y) coordinates and assume the potential profile along the channel axis to be approximately given by the potential profile along that grid line. Given the high resolution of the grid in the second run, this approximation is reasonable. In addition to the table of the potential at all grid points, we also output at the end of this second run a map of the potential (phimap) throughout the system. This map is used to project the potential to the molecular surface of the corresponding channel configuration.

To compute the electrostatic potential energy profile of a test K^+ ion along the axis of a channel structure, we require, in addition to the Coulomb contribution arising from the corresponding potential profile discussed above, a contribution due to the interaction of the test charge with its reaction field, the so-called reaction-field energy or self-energy.[43] To compute the self-energy profile of a K^+ ion along the channel axis of a given configuration, we insert into the corresponding reduced PDB file (see above) a test K^+ ion at the starting position of $z = 35$ Å on the grid line chosen above to approximate the channel axis. For the electrostatic and structural calculations performed here, the channel typically lies in the range from $z = -32$ Å (intracellular side) to $z = 35$ Å (extracellular side). The resulting PDB file is then fed into DelPhi, with all charges except that of the test ion set to zero, and the self-energy of the test ion at $z = 35$ Å is computed. The same DelPhi parameters and strategy are employed as for the potential profile calculation above. The test ion is then moved toward the pore by 1 Å along the channel axis, and the DelPhi self-energy calculation is repeated and so on until $z = 10$ Å is reached. The resulting self-energy profile for the given configuration consists of the self-energy of the test ion evaluated at 26 points separated by 1 Å intervals along the channel axis, between $z = 10$ Å and $z = 35$ Å.

2.4. Structural Calculations. The pore radius along the channel axis of the open and inactive structures of HERG is calculated using the code HOLE.[44] As with the electrostatic potential computations, we first obtain a molecular configuration from either of the two equilibrated systems described in section 2.1, with open or inactive HERG structures and filter occupancy state (1010). We extract from the PDB file of this configuration all water molecules, chloride and potassium ions, and POPE lipid molecules, leaving only the protein in the file. The PDB file is then fed into HOLE to compute the pore radius along the channel axis of the configuration. In the HOLE computations, AMBER values are used for the Van der Waals radii of the protein atoms. In addition to the pore radius, we also compute the molecular surface of the open and inactive structures of HERG. The molecular surface is exploited both for the information it conveys and for mapping the electrostatic potential computed as described above.

3. Results

We first examine the validity of the HERG homology model with free energy calculations of its selectivity. We then explore the possibility of a steric and/or electrostatic mechanism of inactivation, based on structural and electrostatics results.

3.1. Selectivity of the HERG Homology Model. As a means of checking the validity of the HERG homology model, its selectivity property is examined. FEP is used to compute the relative binding free energies $\Delta\Delta G$ of K^+ and Na^+ in the filter sites by means of eq 1. In all FEP calculations, we enforced restrictions (a) and (b) of section 2.2 to obtain accurate results. Specifically, to ensure that the free energy change in each window of any FEP run is less than 2 kT (1.5 kcal/mol), we performed preliminary FEP runs with 20, 40, and 80 equal-sized windows. To ensure good convergence of ensemble averages in each window, various equilibration and sampling times per window were tested. On the basis of these tests, we opted to use 40 windows in any FEP run and 20 ps of equilibration followed by 20 ps of ensemble sampling in each window. Double-ended sampling over the entire run is also used in all FEP runs; thus in what follows $\Delta G(K^+ \rightarrow Na^+)$ represents the average of the free energy differences from a forward and a backward mutation between K^+ and Na^+.

To obtain $\Delta\Delta G$, we first compute the solvation free energy difference of K^+ and Na^+ in bulk water using FEP in a cubic water box with side length 29 Å. We obtain $\Delta G_w(K^+ \rightarrow Na^+) = -20.9$ kcal/mol. FEP calculations of $\Delta G_w(K^+ \rightarrow Na^+)$ with 20 and 80 windows yielded similar values. This value of $\Delta G_w(K^+ \rightarrow Na^+)$, obtained with the CHARMM 27 force field,[34] is consistent with values computed elsewhere with the same force field.[45] Although the CHARMM force field appears to overestimate the experimental value[31] of the solvation free energy difference of K^+ and Na^+ by approximately 3 kcal/mol, error cancellation effects between the computed $\Delta G_p(K^+ \rightarrow Na^+)$ and $\Delta G_w(K^+ \rightarrow Na^+)$ terms in eq 1 should yield accurate values for $\Delta\Delta G$.

Second, we consider two equilibrated systems of HERG corresponding to its open structure with filter occupancy states (1010) and (0101), generated as described in section 2.1. As noted previously, a third K^+ ion is always present in the internal cavity. Experimental and theoretical justifications have been given, for instance, for the inclusion of the K^+ ion in the cavity in FEP calculations involving these filter occupancy states in

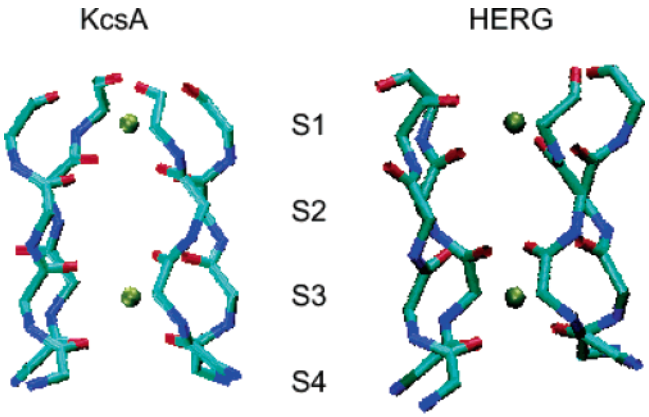

Figure 5. Selectivity filters of KcsA and the HERG homology model after equilibration with K^+ ions occupying the binding sites S1 and S3. The filter of HERG is from the structure corresponding to the open state of the channel. The water molecules in sites S2 and S4 are not shown.

the KcsA potassium channel.[31] To maintain the desired occupancy states during the FEP calculations, harmonic restraints of 10 kcal/mol/Å^2 were applied to the three K^+ ions. For the system with the (1010) occupancy state, the K^+ ion in site S1 is mutated into a Na^+ ion and vice versa to obtain $\Delta G_p^1(K^+ \rightarrow Na^+) = -20.68$ kcal/mol, yielding from eq 1 a relative binding free energy for site S1 of $\Delta\Delta G^1 = 0.22$ kcal/mol. For the system with the (0101) occupancy state, we mutated the K^+ ion in site S2 into a Na^+ ion and vice versa to obtain $\Delta G_p^2(K^+ \rightarrow Na^+) = -15.24$ kcal/mol, yielding a relative binding free energy for site S2 of $\Delta\Delta G^2 = 5.66$ kcal/mol. These $\Delta\Delta G^1$ and $\Delta\Delta G^2$ values imply that the HERG homology model is essentially nonselective in site S1 and strongly selective for K^+ over Na^+ in site S2.

For comparison, we consider also two equilibrated systems of the KcsA potassium channel with filter occupancy states (1010) and (0101), generated as described in section 2.1. FEP calculations are performed on these systems with the same simulation parameter values used for the HERG systems. For the system with the (1010) occupancy state, the K^+ ion in site S1 is mutated into a Na^+ ion and vice versa to obtain $\Delta G_p^1(K^+ \rightarrow Na^+) = -16.6$ kcal/mol, yielding from eq 1 a relative binding free energy for site S1 of $\Delta\Delta G^1 = 4.3$ kcal/mol. For the system with the (0101) occupancy state, the K^+ ion in site S2 is mutated into a Na^+ and vice versa to obtain $\Delta G_p^2(K^+ \rightarrow Na^+) = -17.55$ kcal/mol, yielding a relative binding free energy for site S2 of $\Delta\Delta G^2 = 3.35$ kcal/mol. These values of $\Delta\Delta G^1$ and $\Delta\Delta G^2$ imply that the KcsA channel, in either occupancy state, is highly selective for K^+ over Na^+ and are consistent with the values computed by Luzhkov and Aqvist.[31]

The result that the HERG homology model is nonselective in site S1 is in contrast to other potassium channels, which (like KcsA above) are strongly selective for K^+ at all binding sites. However, this lack of selectivity in site S1 of the HERG model is consistent with the experimental observation that HERG channels, unlike other voltage-gated potassium channels, are blocked by extracellular Na^+.[46] The contrast in the selectivity of the S1 site between KcsA and the HERG model can be interpreted by comparing the structures of their filters in the equilibrated systems used in the FEP calculations. As seen in Figure 5, the S2−S4 sites are structurally very similar in both filters, but the S1 site displays a much more open structure in HERG. Consequently this site is not selective for K^+ ions in the HERG model. These findings on the selectivity of the HERG homology model suggest that it is a reliable starting point for studies of inactivation in HERG, and possible improvement and refinement of the model are worth pursuing.

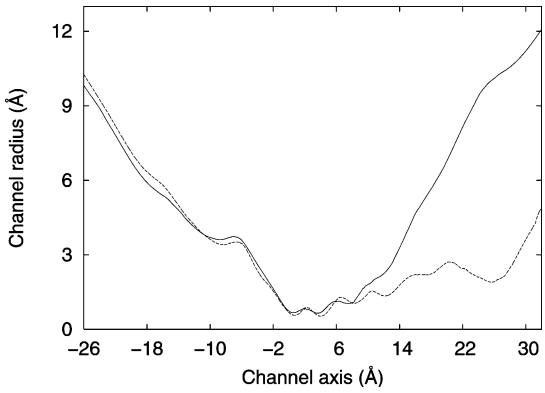

Figure 6. Average pore radius for the open (solid) and inactive (dashed) states of HERG along the central axis of the channel. The channel is in the (1010) filter occupancy state.

3.2. Steric Mechanism for Inactivation. Figure 4 shows the structures of the open and inactive states of the HERG homology model with filter occupancy state (1010), obtained after the equilibration described in section 2.1. The initial homology structures for the open and inactive states employ the helical structures for the S5-P linkers, as determined from the NMR experiments.[17,19] As seen in Figure 4, this feature is partially lost after equilibration. More importantly, in the initial homology structures, the S5-P linkers are closer to the pore axis in the inactive state than in the open one. This contrast becomes even greater in Figure 4, as the S5-P linkers move during equilibration much further away from the channel axis in the open state than in the inactive one. This effect can also be inferred from Figure 3, which shows the rmsd from the initial configurations of HERG, for the open and inactive structures during equilibration. In the top panel all of the backbone atoms in the HERG model are included in the calculation, while in the bottom panel only the backbone atoms in the S5-P linker are included. It is clear from the bottom panel that the S5-P linkers exhibit a more dynamic behavior in the open state and a comparatively more stable behavior in the inactive one.

To give a more quantitative measure of this structural difference between the S5-P linkers of the open and inactive states, we calculate the pore radius along the channel axis of the open and inactive equilibrated structures of HERG. To have a sufficient sampling of the open and inactive structures, we run MD simulations on the corresponding equilibrated systems of section 2.1 with filter occupancy state (1010) and generate 10 configurations from each system, with successive configurations separated by a time interval of 20 ps. The pore radius along the channel axis of each configuration is then computed with the HOLE program as detailed in section 2.4. The 10 results corresponding to either the open or the inactive structure of HERG are then smoothed with natural cubic splines and averaged to generate an average pore radius versus channel axis plot for each structure. The average pore radius plots for the open and inactive states of HERG are shown in Figure 6. Recall that the channel lies roughly in the range from $z = -32$ Å (intracellular side) to $z = 35$ Å (extracellular side). As anticipated, the open state displays a much larger average pore radius at the extracellular pore entrance than the inactive state. The observation that the S5-P linkers are much closer to the pore axis in the inactive state, and thus might create a steric hindrance for permeating K^+ ions, suggests the possibility of a steric mechanism for inactivation in the HERG homology model.

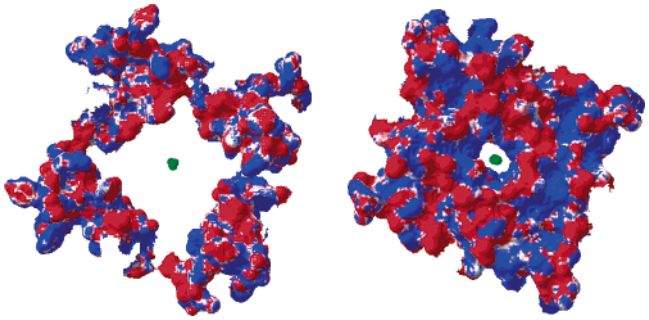

Figure 7. Electrostatic potential mapped to the molecular surfaces associated with the S5-P linkers shown in the top panels of Figure 4. As in Figure 4, the left and right images correspond to the open and inactive states in HERG after equilibration with K^+ ions (lime) in sites S1, S3, and the internal cavity. The molecular surfaces associated with the pore helices in the top panels of Figure 4 are not displayed. Zero potentials appear in white. Positive potentials range in color transparency from white to blue, with potentials greater than or equal to 2 kT/*e* shown in blue. Negative potentials range in color transparency from white to red, with potentials smaller than or equal to −2 kT/*e* shown in red.

Further appreciation of this possibility can be obtained by examining the molecular surface of the channel. To this end, we select from the pair of 10 equilibrated configurations mentioned above, one configuration corresponding to the open HERG state and another to the inactive state. For convenience, the two configurations used to generate Figure 4 are chosen. Next we compute the molecular surface of each configuration and display in Figure 7 only that part of the surface associated with the S5-P linkers in the top panels of Figure 4. The sharp contrast between the open geometry of the molecular surface at the extracellular pore entrance in the open state and the narrow restrictive geometry of the corresponding surface in the inactive state strongly hints at the feasibility of a steric barrier mechanism for inactivation, mediated by the S5-P linkers. Calculations of the molecular surface with other equilibrated configurations yield similar contrasting features between the open and the inactive HERG states.

3.3. Electrostatic Mechanism for Inactivation. To determine the viability of an electrostatic mechanism for inactivation in the HERG homology model, we examine three electrostatic quantities in both the open and the inactive structures of HERG: the electrostatic potential profile along the channel axis, the electrostatic potential mapped to the molecular surfaces of section 3.2, and the electrostatic potential energy profile of a test K^+ ion entering the channel from the extracellular side along the channel axis. To obtain the potential profiles and have a sufficient sampling of the open and inactive structures we use the same 10 configurations generated from the corresponding equilibrated systems for the pore radii calculations described above. The electrostatic potential profile along the channel axis of each configuration is computed with the DelPhi program as detailed in section 2.3. The 10 potential profiles corresponding to either the open or the inactive structure of HERG are then smoothed and averaged to generate an average potential profile along the channel axis of each structure. The average electrostatic potential profiles for the open and inactive states of HERG are shown in Figure 8 and correspond to the average pore radii plots in Figure 6. Figure 8 shows an electrostatic barrier of approximately 8 kT/*e* around $z = 18$ Å at the channel extracellular entrance in the inactive state. This barrier hints at the likelihood of an electrostatic mechanism for inactivation in the HERG homology model.

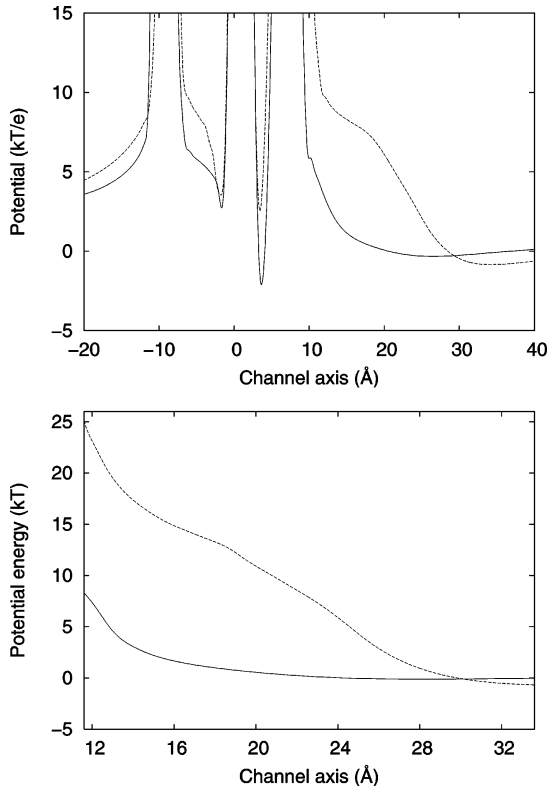

Figure 8. (Top) Average electrostatic potential profiles along the central axis of the HERG channel. (Bottom) Average electrostatic potential energy profiles of a test K^+ ion along the channel axis. The channel is in the (1010) filter occupancy state. In both panels the solid lines correspond to the open state of HERG, and the dashed lines correspond to the inactive state.

As with assessing the possibility of a steric mechanism for inactivation, additional appreciation of the possibility of an electrostatic mechanism is achieved by examining the electrostatic potential evaluated at the molecular surfaces from section 3.2 by means of the potential maps computed as described in section 2.3. Figure 7 shows the electrostatic potential mapped to the molecular surfaces and color-coded by value with cutoffs at 2 kT/*e* and −2 kT/*e*. The immediate narrow region of the molecular surface defining the extracellular pore entrance in the inactive HERG state is almost entirely the source of a positive potential greater than or equal to 2 kT/*e*, thus contributing to the presence of a potential barrier in the inactive state of Figure 8. By contrast, the region of the corresponding molecular surface defining the extracellular pore entrance in the open state is both geometrically open (i.e., far from the channel axis) and a mixture of patches of positive and negative potentials. Both factors contribute to the absence of a potential barrier in the open state of Figure 8. Again, calculations of the electrostatic potential mapped to the molecular surface with other equilibrated configurations yield similar contrasting features between the open and the inactive HERG states.

To obtain the electrostatic potential energy profile of a test K^+ ion along the channel axis of the open or inactive structure of HERG, the self-energy profile of the test ion along the axis is computed first. To this end, we use the same 10 equilibrated configurations for the open or inactive structures as in the potential profile calculations above. The self-energy profile of a test K^+ ion along the channel axis of each configuration is computed with DelPhi as described in section 2.3. The 10 self-energy profiles corresponding to either the open or the inactive structure of HERG are then averaged, and the result is smoothed to generate an average self-energy profile (not shown here) along

the channel axis of each structure in the *z*-range of 10−35 Å. Multiplication of the average potential profiles in Figure 8 by the test ion charge (here simply 1*e*) leads to corresponding average Coulomb energy profiles of a K^+ ion along the channel axis. Finally, the average self-enegy profile for the open or inactive structure of HERG is added to the corresponding average Coulomb energy profile to give an average potential energy profile of a test K^+ ion approaching the channel pore from the extracellular side along the channel axis, as shown in Figure 8. As expected,[43] inclusion of the self-energy enhances the potential energy barrier encountered in the inactive state by a K^+ ion entering from the extracellular side. The barrier is increased from its 8 kT Coulomb value to a total value of approximately 14 kT, around $z = 18$ Å. The potential energy barrier in the inactive state, which could prevent the permeation of K^+ ions, again points to a possible contribution of an electrostatic mechanism to inactivation in the HERG homology model.

4. Discussion

There are two leading mechanisms for explaining the fast inactivation in HERG: (a) Conformational changes in the S5-P linker create a steric and/or electrostatic barrier blocking the conduction pathway, or (b) conformational changes in the selectivity filter induced by the motion of the S5-P linker shut down the filter. Of course, a combination of (a) and (b) operating in tandem is also possible. Here we have focused on studying the feasibility of mechanism (a) by means of MD simulations, structural and continuum electrostatics calculations, performed on a homology model of the HERG channel, which assigns specific conformations to the S5-P linkers in the open and inactive states.

Our HERG selectivity results, obtained with FEP calculations of the relative binding free energies of Na^+ and K^+ to the channel pore, show that the HERG homology model is nonselective for K^+ in site S1 but strongly selective for it in site S2. These results are in contrast to the KcsA selectivity results obtained with FEP here and elsewhere,[31,47] which imply that both sites S1 and S2 are highly selective for K^+ in KcsA. The situation is similar for other potassium channels. However, our HERG results are entirely consistent with the known inhibition of HERG channels by extracellular Na^+. The similarity between the binding affinities for Na^+ and K^+ at site S1 in HERG means that Na^+ can compete for K^+ binding at S1 but cannot then permeate as it has a very low affinity at S2. Thus Na^+ acts as a blocker in HERG.[46]

Given the close correlation between our HERG selectivity results and the published experimental data, we feel confident that the HERG homology model is a reasonable starting point for inactivation studies. The subsequent structural and electrostatics arguments, based on this homology model, suggest that mechanism (a) contributes to inactivation in HERG. However, we cannot rule out the possibility given in (b) that inactivation may be a two-step process, and conformational changes in the selectivity filter may also contribute to inactivation. The observation that mutation of Ser620 (located at the C-terminal end of the pore helix) to threonine abolishes inactivation clearly suggests that conformational changes within the pore helix and/or selectivity filter are likely to be involved in inactivation.[13] Additionally, in most K_V channels, the tyrosine in the selectivity filter and the two tryptophans in the pore helix are thought to provide a hydrogen bond network that stabilizes the selectivity filter.[20,48−50] In HERG, there is a phenylalanine rather than a tyrosine in the selectivity filter and a tyrosine and phenylalanine rather than two tryptophans in the pore helix,[18] thereby eliminating any possibility of a hydrogen bond network. It has therefore often been suggested that this would make the HERG selectivity filter more flexible and prone to collapse.[51] Recently, Gang and Zhang have shown that the inactivated state of HERG does appear to involve collapse of the selectivity filter.[52] However, the precise molecular basis of this collapse remains to be determined. Given that mutations in the selectivity filter and pore helix are usually nonfunctional, this question will be difficult to address experimentally. An alternative strategy for examining this problem is to use a computational modeling approach. The results presented here suggest that the HERG homology model, developed by Tseng and Guy[29] and adopted here, is suitable for pursuing this strategy in future studies.

Acknowledgment. This work was supported by grants from the Australian Research Council. J.I.V. is a National Health and Medical Research Council R. D. Wright Fellow. Calculations were carried out using the Barossa cluster at the Australian Center for Advanced Computing and Communications. We thank Dr. Robert Guy for providing the initial homology model for the HERG channel.

References and Notes

(1) Sanguinetti, M. C.; Jiang, C.; Curran, M. E.; Keating, M. T. A mechanistic link between an inherited and an acquired cardiac arrhythmia: HERG encodes the I_{Kr} potassium channel. *Cell* **1995**, *81*, 299−307.

(2) Smith, P. L.; Baukrowitz, T.; Yellen, G. The inward rectification mechanism of the HERG cardiac potassium channel. *Nature* **1996**, *379*, 833−836.

(3) Spector, P. S.; Curran, M. E.; Zou, A.; Keating, M. T.; Sanguinetti, M. C. Fast inactivation causes rectification of the I_{Kr} channel. *J. Gen. Physiol.* **1996**, *107*, 611−619.

(4) Tseng, G. N. I_{Kr}: The HERG channel. *J. Mol. Cell. Cardiol.* **2001**, *33*, 835−849.

(5) Curran, M. E.; Splawski, I.; Timothy, K. W.; Vincent, G. M.; Green, E. D.; Keating, M. T. A molecular basis for cardiac arrhythmia: HERG mutations cause long QT syndrome. *Cell* **1995**, *80*, 795−803.

(6) Brugada, R.; Hong, K.; Dumaine, R.; Cordeiro, J.; Gaita, F.; Borggrefe, M.; Menendez, T. M.; Brugada, J.; Pollevick, G. D.; Wolpert, C.; Burashnikov, E.; Matsuo, K.; Wu, Y. S.; Guerchicoff, A.; Bianchi, F.; Giustetto, C.; Schimpf, R.; Brugada, P.; Antzelevitch, C. Sudden death associated with short-QT syndrome linked to mutations in HERG. *Circulation* **2004**, *109*, 30−35.

(7) Vandenberg, J. I.; Walker, B. D.; Campbell, T. J. HERG K^+ channels: Friend and foe. *Trends Pharmacol. Sci.* **2001**, *22*, 240−246.

(8) Pearlstein, R.; Vaz, R.; Rampe, D. Understanding the structure−activity relationship of the HERG cardiac K^+ channel. A model for bad behavior. *J. Med. Chem.* **2003**, *46*, 2017−2022.

(9) Yellen, G. The moving parts of voltage-gated ion channels. *Q. Rev. Biophys.* **1998**, *31*, 239−95.

(10) Vandenberg, J. I.; Torres, A. M.; Campbell, T. J.; Kuchel, P. W. The HERG K^+channel: Progress in understanding the molecular basis of its unusual gating kinetics. *Eur. Biophys. J.* **2004**, *33*, 89−97.

(11) Piper, D. R.; Varghese, A.; Sanguinetti, M. C.; Tristani-Firouzi, M. Gating currents associated with intra-membrane charge displacement in HERG potassium channels. *Proc. Nat. Acad. Sci. U.S.A.* **2003**, *100*, 10534−10539.

(12) Smith, P. L.; Yellen, G. Fast and slow voltage sensor movements in HERG potassium channels. *J. Gen. Physiol.* **2002**, *119*, 275−293.

(13) Ficker, E.; Jarolimek, W.; Kiehn, J.; Baumann, A.; Brown, A. M. Molecular determinants of dofetilide block of HERG K^+ channels. *Circ. Res.* **1998**, *82*, 386−395.

(14) Herzberg, I. M.; Trudeau, M. C.; Robertson, G. A. Transfer of rapid inactivation and sensitivity to the class III antiarrhythmic drug E-4031 from HERG to M-eag channels. *J. Physiol.* **1998**, *511*, 3−14.

(15) Schonherr, R.; Heinemann, S. H. Molecular determinants for activation andinactivation of HERG, a human inward rectifier potassium channel. *J. Physiol.* **1996**, *493*, 635−642.

(16) Liu, J.; Zhang, M.; Jiang, M.; Tseng, G. N. Structural and functional role of theextracellular S5-P linker in the HERG potassium channel. *J. Gen. Physiol.* **2002**, *120*, 723−737.

(17) Torres, A. M.; Bansal, P. S.; Sunde, M.; Clarke, C. E.; Bursill, J. A.; Smith, D. J.; Bauskin, A.; Breit, S. N.; Campbell, T. J.; Alewood, P.; Kuchel, P. W.; Vandenberg, J. I. Structure of the HERG K^+ channel S5-P

extracellular linker: Role of anamphipathic α-helix in C-type inactivation. *J. Biol. Chem.* **2003**, *278*, 42136−42148.

(18) Trudeau, M.; Warmke, J.; Ganetzky, B.; Robertson, G. HERG, a human inward rectifier in the voltage-gated potassium channel family. *Science* **1995**, *269*, 92−95.

(19) Jiang, M.; Zhang, M.; Maslennikov, I. V.; Liu, J.; Wu, D. M.; Korolkova, Y. V.; Arseniev, A. S.; Grishin, E. V.; Tseng, G. N. Dynamic conformational changes of extracellular S5-P linkers in the hERG channel. *J. Physiol.* **2005**, *569*, 75−89.

(20) Doyle, D. A.; Cabral, J. M.; Pfuetzner, R. A.; Kuo, A.; Gulbis, J. M.; Cohen, S. L.; Chait, B. T.; MacKinnon, R. The structure of the potassium channel: Molecular basis of K^+ conduction and selectivity. *Science* **1998**, *280*, 69−77.

(21) Zhou, Y.; Morais-Cabral, J. H.; Kaufman, A.; MacKinnon, R. Chemistry of ioncoordination and hydration revealed by a K^+ channel−Fab complex at 2.0 Å resolution. *Nature* **2001**, *414*, 43−48.

(22) Jiang, Y.; Lee, A.; Chen, J.; Cadane, M.; Chait, B. T.; MacKinnon, R. Crystal structure and mechanism of a calcium-gated potassium channel. *Nature* **2002**, *417*, 515−522.

(23) Jiang, Y.; Lee, A.; Chen, J.; Ruta, V.; Cadane, M.; Chait, B. T.; MacKinnon, R. X-ray structure of a voltage-dependent K^+ channel. *Nature* **2003**, *423*, 33−41.

(24) Mitcheson, J. S.; Chen, J.; Lin, M.; Culberson, C.; Sanguinetti, M. C. A structural basis for drug-induced long QT syndrome. *Proc. Natl. Acad. Sci. U.S.A.* **2000**, *97*, 12329−12333

(25) Rajamani, R.; Tounge, B. A.; Li, J.; Reynolds, C. H. A two-state homology model of HERG K^+ channel: Application to ligand binding. *Bioorg. Med. Chem. Lett.* **2005**, *15*, 1737−1741.

(26) Pearlstein, R. A.; Vaz, R. J.; Kang, J.; Chen, X.; Preobrazhenskaya, M.; Shchekotihin, A. E.; Korolev, A. M.; Lysenkova, L. N.; Miroshinkova, O. L.; Hendrix, J.; Rampe, D. Characterization of HERG potassium channel inhibition using 3D QSAR and homology modeling approaches. *Bioorg. Med. Chem. Lett.* **2003**, *13*, 1829−1835.

(27) Osterberg, F.; Aqvist, J. Exploring blocker binding to a homology model of theopen HERG K^+ channel using docking and molecular dynamics methods. *FEBS Lett.* **2005**, *579*, 2939−2944.

(28) Farid, R.; Day, T.; Friesner, R. A.; Pearlstein, R. A. New insights about HERG blockade obtained from protein modeling, potential energy mapping, and docking studies. *Bioorg. Med. Chem.* **2006**, *14*, 3160−3173.

(29) Tseng, G. N.; Guy, H. R. Structure−function studies of outer mouth and voltage sensor domain of HERG. *Novartis Found. Symp.* **2005**, 266 19−43.

(30) Humphrey, W.; Dalke, A.; Schulten, K. VMD−Visual molecular dynamics. *J. Mol. Graphics* **1996**, *14*, 33−38.

(31) Luzhkov, V. B.; Aqvist, J. K^+/Na^+ selectivity of the KcsA potassium channel from microscopic free energy perturbation calculations. *Biochim. Biophys. Acta* **2001**, *1548*, 194−202.

(32) Weber, W.; Hunenberger, P. H.; McCammon, J. A. Molecular dynamics simulations of apolyalanine octapeptide under Ewald boundary conditions: Influence of artifical periodicity on peptide conformation. *J. Phys. Chem. B* **2000**, *104*, 3668−3675.

(33) Kale, L.; Skeel, R.; Bhandarkar, M.; Brunner, R.; Gursoy, A.; Krawetz, N.; Phillips, J.; Shinozaki, A.; Varadarajan, K.; Schulten, K. NAMD2: Greater scalability for parallel molecular dynamics. *J. Comput. Phys.* **1999**, *151*, 283−312.

(34) MacKerell, A. D., Jr.; Bashford, D.; Bellott, R. L.; Dunbrack, R. L., Jr.; Evanseck, J. D.; Field, M. J.; Fischer, S.; Gao, J.; Guo, H.; Ha, S.; Joseph-McCarthy, D.; Kuchnir, L.; Kuczera, K.; Lau, F. T. K.; Mattos, C.; Michnick, S.; Ngo, T.; Nguyen, D. T.; Prodhom, B.; Reiher, W. E., III; Roux, B.; Schlenkrich, M.; Smith, J. C.; Stote, R.; Straub, J.; Watanabe, M.; Wiorkiewicz-Kuczera, J.; Yin, D.; Karplus, M. All-atom empirical potential for molecular modeling and dynamics studies of proteins. *J. Phys. Chem. B* **1998**, *102*, 3586−3616.

(35) Feller, S.; Zhang, Y.; Pastor, R.; Brooks, B. Constant pressure molecular dynamics: The Langevin piston method. *J. Chem. Phys.* **1995**, *103*, 4613−4621.

(36) Nagle, J. F.; Tristram-Nagle, S. Structure of lipid bilayers. *Biochim. Biophys. Acta* **2000**, 1469, 159−195.

(37) Beveridge, D. L.; DiCapua, F. M. Free energy via molecular simulation: Applications to chemical and biomolecular systems. *Annu. Rev. Biophys. Biophys. Chem.* **1989**, *18*, 431−492.

(38) King, P. M. Free energy via molecuar simulation: A primer. In *Computer Simulation of Biomolecular Systems: Theoretical and Experimental Applications*; van Gunsteren, W. F., Weiner, P. K., Wilkinson, A. J., Eds.; ESCOM: Leiden, The Netherlands, 1993; Vol. 2, pp 267−314.

(39) Pearlman, D. A.; Kollman, P. A. Free energy perturbation calculations: Problems and pitfalls along the gilded road. In *Computer Simulation of Biomolecular Systems: Theoretical and Experimental Applications*; van Gunsteren, W. F., Weiner, P. K., Eds.; ESCOM: Leiden, The Netherlands, 1989; pp 101−119.

(40) Rocchia, W.; Alexov, E.; Honig, B. Extending the applicability of the nonlinear Poisson−Boltzmann equation: Multiple dielectric constants and multivalent ions. *J. Phys. Chem. B* **2001**, *105*, 6507−6514.

(41) Rocchia, W.; Sridharan, S.; Nicholls, A.; Alexov, E.; Chiabrera, A.; Honig, B. Rapid grid-based construction of the molecular surface and the use of induced surface charge to calculate reaction field energies: Applications to the molecular systems and geometric objects. *J. Comput. Chem.* **2002**, *23*, 128−137.

(42) Gilson, M. K.; Sharp, K. A.; Honig, B. H. Calculating the electrostatic potential of molecules in solution−Method and error assessment. *J. Comput. Chem.* **1988**, *9*, 327−335.

(43) Kuyucak, S.; Andersen, O. S.; Chung, S. H. Models of permeation in ion channels. *Rep. Prog. Phys.* **2001**, *64*, 1427−1472.

(44) Smart, O. S.; Goodfellow, J. M.; Wallace, B. A. The pore dimensions of gramicidin A. *Biophys. J.* **1993**, *65*, 2455−2460.

(45) Bernèche, S.; Roux, B. Energetics of ion conduction through the K^+ channel. *Nature* **2001**, *414*, 73−77.

(46) Numaguchi, H.; Johnson, J. P.; Petersen, C. I.; Balser, J. R. A sensitive mechanism for cation modulation of potassium current. *Nat. Neurosci.* **2000**, *3*, 429−430.

(47) Aqvist, J.; Luzhkov, V. Ion permeation mechanism of the potassium channel. *Nature* **2000**, *404*, 881−884.

(48) Ranganathan, R.; Lewis, J. H.; MacKinnon, R. Spatial localization of the K^+ channel selectivity filter by mutant cycle-based structure analysis. *Neuron* **1996**, *16*, 131−139.

(49) Harris, R. E.; Larsson, H. P.; Isacoff, E. Y. A permanent ion binding site located between two gates of the Shaker K^+ channel. *Biophys. J.* **1998**, *74*, 1808−1820.

(50) Perozo, E.; MacKinnon, R.; Bezanilla, F.; Stefani, E. Gating currents from a nonconducting mutant reveal open−closed conformations in Shaker K^+ channels. *Neuron* **1993**, *11*, 353−358.

(51) Fan, J. S.; Jiang, M.; Dun, W.; McDonald, T. V.; Tseng, G. N. Effects of outer mouth mutations on hERG channel function: A comparison with similar mutations in the Shaker channel. *Biophys. J.* **1999**, *76*, 3128−3140.

(52) Gang, H.; Zhang, S. Na^+ permeation and block of hERG potassium channels. *J. Gen. Physiol.* **2006**, *128*, 55−71.